A Bottom-Up Approach to Build 3D Architectures from Nanosheets for Superior Lithium Storage

Yongji Gong, Shubin Yang, Liang Zhan, Lulu Ma, Robert Vajtai, and Pulickel M. Ajayan**

Two-dimensional (2D) atomic layers such as graphene, and metal chalcogenides have recently attracted tremendous attention due to their unique properties and potential applications. Unfortunately, in most cases, the free-standing nanosheets easily re-stack due to their van der Waals forces, and lose the advantages of their separated atomic layer state. Here, a bottom-up approach is developed to build three-dimensional (3D) architectures by 2D nanosheets such as MoS_2 and graphene oxide nanosheets as building blocks, the thin nature of which can be well retained. After simply chemical reduction, the resulting 3D MoS_2-graphene architectures possess high surface area, porous structure, thin walls and high electrical conductivity. Such unique features are favorable for the rapid diffusions of both lithium ions and electrons during lithium storage. As a consequence, MoS_2-graphene electrodes exhibit high reversible capacity of ≈1200 mAh g^{-1}, with very good cycling performance. Moreover, such a simple and low-cost assembly protocol can provide a new pathway for the large-scale production of various functional 3D architectures for energy storage and conversions.

1. Introduction

Two-dimensional (2D) nanomaterials have long been regarded as attractive materials owing to their unique properties[1,2] and promising applications.[3–6] In particular, recent investigations of graphene have demonstrated their exceptional physical properties including ultrahigh surface area,[7–10] high electron mobility[11] and ballistic transport[12] and others.[13,14] This has triggered a keen interest in 2D atomic layers (termed as nanosheets from now on in this context) other than carbon, such as nitrides,[15,16] oxides,[6,17] and sulfides.[18,19] Until now, nanosheets of various compositions have been studied, made by procedures including scotch tape based micromechanical exfoliation,[20,21] chemical vapor deposition,[22] epitaxial growth,[23,24] and liquid exfoliation.[18,25] Among them, the liquid exfoliation of layered materials provides an efficient approach to produce bulk amounts of free-standing nanosheets.[18,25] However, the exfoliated nanosheets would re-aggregate or re-stack easily due to their van der Waals forces when they are extracted from suspensions.[3,26] As a result, the advantages of the separated nanosheets disappear, leading to significantly different properties that are characteristic for isolated atomic layers.[3,26] Taking the application of electrochemically active nanosheets for lithium storage as an example, the diffusion time t of lithium ions in electrode materials is proportional to the square of the diffusion length L ($t = L^2/D$),[27,28] thus the re-stacking of nanosheets undoubtedly significantly influences their electrochemical performances.

In this work, we demonstrate a bottom-up approach to construct three-dimensional (3D) architectures by employing the 2D nanosheets of MoS_2 and graphene oxide (GO) as co-building blocks via their conctrollable assembly properties. After simple chemical reduction, the 3D MoS_2-graphene architectures can be achieved. The resulting 3D MoS_2-graphene architectures not only possess high surface area, multilevel porous structure and thin walls, but also show high electrical conductivity. Such unique features can provide numerous channels for the access of electrolyte and facilitate the ultrafast diffusion of lithium ions during the cycling processes, and at the same time, are favorable for the fast electron transport in the electrode. As a consequence, the optimal MoS_2-graphene architecture exhibit a very high capacity of 1220 mAh g^{-1}, with excellent cycling performance for lithium storage.

2. Results and Discussion

2.1. Preparation and Characterization of MoS_2 and Graphene Sheets Co-Constructed 3D Architectures

The overall synthetic procedure of MoS_2 and graphene sheets co-constructed 3D architectures involves three steps: MoS_2 nanosheets were firstly fabricated via liquid exfoliation of commercially available bulk MoS_2, and GO were produced by the modified Hummers method from flake graphite.[29,30] The resulting MoS_2 and GO nanosheets were then employed as building blocks to co-assemble at a constant temperate of

Y. J. Gong, Prof. P. M. Ajayan
Department of Chemistry
Rice University
6100 Main Street, Houston 77005, TX, USA
E-mail: ajayan@rice.edu
Dr. S. B. Yang, L. Zhan, L. L. Ma, R. Vajtai,
Prof. P. M. Ajayan
Department of Mechanical Engineering & Materials Science
Rice University
6100 Main Street, Houston 77005, TX, USA
E-mail: sy13@rice.edu

DOI: 10.1002/adfm.201300844

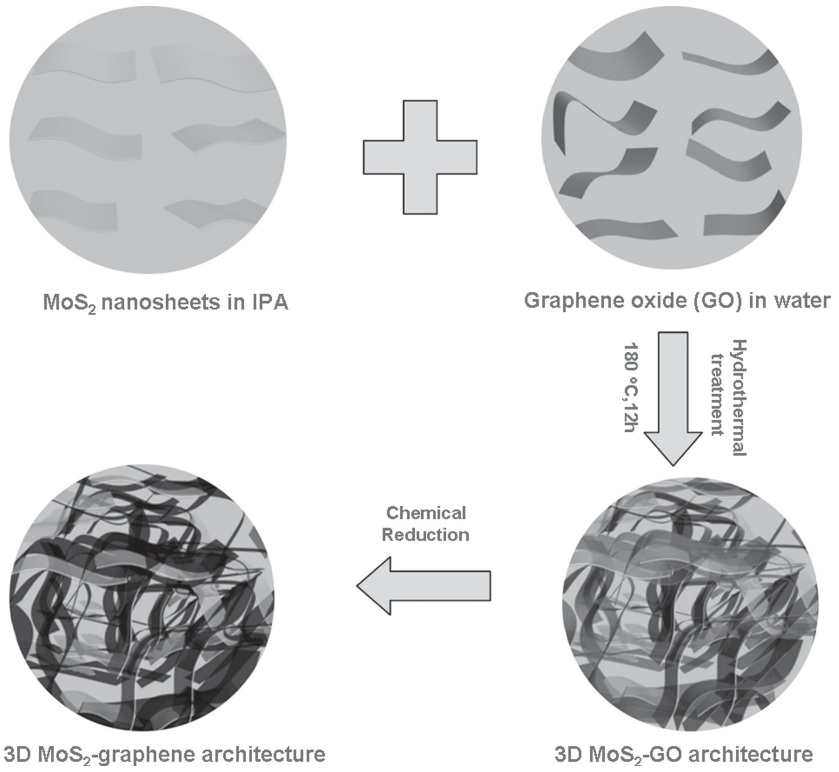

Figure 1. Schematic illustration for the construction of 3D MoS_2-graphene architectures. It mainly involves three steps: (1) fabrication of MoS_2 and graphene oxide nanosheets via liquid exfoliation and Hummers methods, respectively; (2) hydrothermal treatment of the mixed dispersion of MoS_2 and GO nanosheets in IPA (Isopropyl alcohol)/water (1:2, v/v) at 180 °C for 12 h; (3) chemical reduction of GO to generate 3D MoS_2-graphene architectures.

180 °C in a Teflon-lined autoclave, where the mixed solvents of water and IPA (Isopropyl alcohol) (2:1, v/v) were used for the homogeneous dispersions of both nanosheets (**Figure 1**, for details, see Experimental Section). Notably, the content of MoS_2 nanosheets in the as-prepared architectures was readily tunable by simply adjusting the ratio of MoS_2 to GO (four ratios of (9:1, 5.7:1, 4:1 and 1.5:1 were chosen in this context) during the synthesis process. Finally, GO in the resulting samples was chemically reduced to graphene (reduced graphene oxide), giving rise to MoS_2-graphene architectures with different MoS_2 content (Figure S1 in the Supporting Information).

The morphology and microstructure of as-prepared MoS_2 and graphene oxide nanosheets were firstly investigated via scanning electron microscopy (SEM) and transmission electron microscopy (TEM). Apparently, abundant thin and transparent nanosheets are obtained (**Figure 2** and Supporting Information Figure S2), similar to those reported for MoS_2 and graphene oxide sheets.[18,26] The lateral sizes of these nanosheets were typically in the range from 100 to 3000 nm for MoS_2, and from 500 nm to several micrometers for graphene oxide. In comparison, the single-crystalline MoS_2 nanosheets (Figure 2 and Supporting Information Figure S3) are more rigid than graphene oxide sheets, whose wrinkled feature may originate from the defective structures formed during the fabrication process or/and from their intrinsic flexible nature.[31]

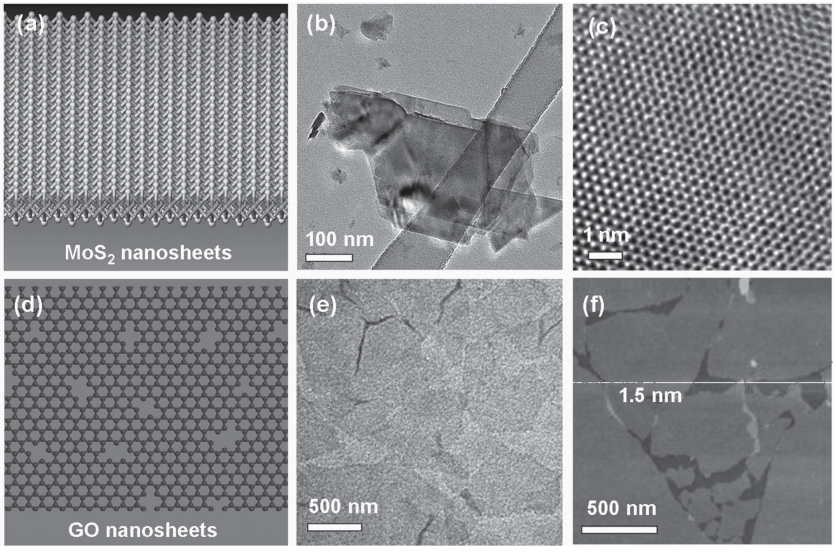

Figure 2. 2D nanosheets including MoS_2 and graphene oxide nanosheets. a) Structural model of atomic layers of MoS_2, b) TEM, and c) HRTEM images of MoS_2 nanosheets, showing the single crystalline structure. d) Structural model of graphene oxide nanosheet, e) TEM and f) AFM images of graphene oxide nanosheets, suggesting uniform thickness of about 1.5 nm.

Cross-sectional atomic force microscopy (AFM) was conducted to further investigate the structural features of the resulting nanosheets. Their typical AFM image and thickness analyses (Figure 2) reveal the same morphology as the observations from SEM and TEM, with uniform thicknesses of ≈2 nm for both MoS_2 and graphene oxide nanosheets. Associated with analysis of flake-edge from high resolution TEM (HRTEM) of MoS_2 nanosheet (Supporting Information Figure S3), the coexistence of mono- and few-layer nanosheets are demonstrated. The stoichiometric compositions of MoS_2 (S/Mo = 1.98) nanosheets were clearly confirmed by X-ray photoelectron spectroscopy (XPS) (See Supporting Information Figure S4).

Thus, MoS_2 and graphene oxide nanosheets have been available as building blocks to construct 3D functional architectures. As shown in **Figure 3**, the as-prepared MoS_2-graphene architectures possess a 3D structure with interconnected pores ranging from several nanometers to several micrometers. Moreover, the thin and rigid MoS_2 nanosheets can be clearly observed and homogeneously confined in the frameworks, which efficiently hamper

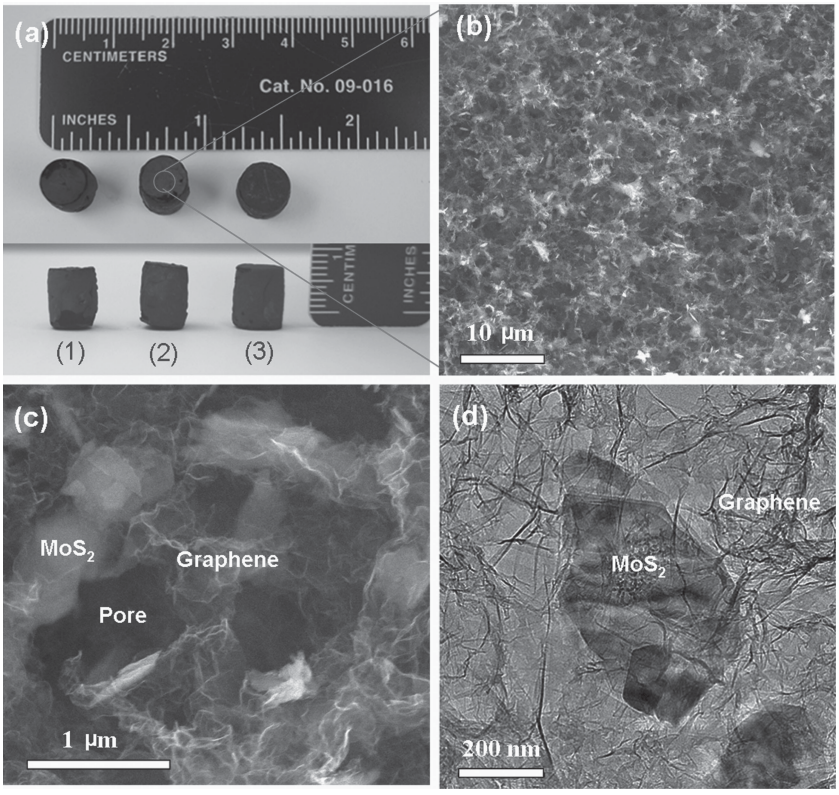

Figure 3. 3D MoS_2-graphene architectures. a) Photographs of MoS_2-graphene architectures with different concentration of MoS_2 nanosheets after chemical reduction and dryness; (1) and (2) 84% and (3) 73%. b,c) Typical SEM images of MoS_2-graphene architecture (84%) with different magnifications, which reveal the porous structure and thin walls containing both MoS_2 and graphene nanosheets. d) TEM image of MoS_2-graphene architecture (84%), showing that MoS_2 nanosheets are confined in the matrix of graphene.

their aggregation and restacking as we expected. This can be further confirmed by their X-ray diffraction (XRD) patterns of MoS_2-graphene architecture (**Figure 4**a), where the intensity of (002) peak characteristic to the layers stacking become very weak with respect to that of the directly dried MoS_2 nanosheet sample. The partial overlapping or coalescing of flexible nanosheets should originate from the cross-linking of the functional groups in graphene sheets (Figure 3c,d), similar to those reported for pure graphene oxide and graphene hydrogels.[32–34] In addition, with increasing the ratios between MoS_2 and graphene oxide sheets during synthesis process, the content of MoS_2 nanosheets in composites clearly increases and the more exfoliated MoS_2 nanosheets are restacked as shown in Supporting Information Figure S5. Pure MoS_2 architecture cannot be built by using MoS_2 nanosheets alone. Thus, it is clear that the abundant functional groups and inherent flexibility of graphene oxide sheets are crucial for constructing the 3D hybrid architectures.

The porous nature of MoS_2-graphene architecture is further validated by nitrogen physisorption measurements. Their adsorption–desorption isotherms exhibit a typical II hysteresis loop at a relative pressure between 0.45 and 0.99 (Figure 4b), characteristic to pores with different pore sizes.[3] Barrett–Joyner–Halenda (BJH) calculations disclose that the pore size distribution is in the range of 2–60 nm, except for the open macropores estimated from the SEM and TEM images. A high specific surface area of up to 202 $m^2\ g^{-1}$ is observed for MoS_2-graphene architecture, which is much higher than those for directly dried MoS_2 nanosheets (42 $m^2\ g^{-1}$) and bulk MoS_2 (23 $m^2\ g^{-1}$). In combination with the analysis based on SEM and TEM images, it is reasonable to believe that the high surface areas of 3D architectures are originated from the thin nanosheets, which give rise to the multilevel porous structures. These unique porous structures can greatly facilitate the access of electrolyte and the fast diffusion of lithium ions during lithium storage.

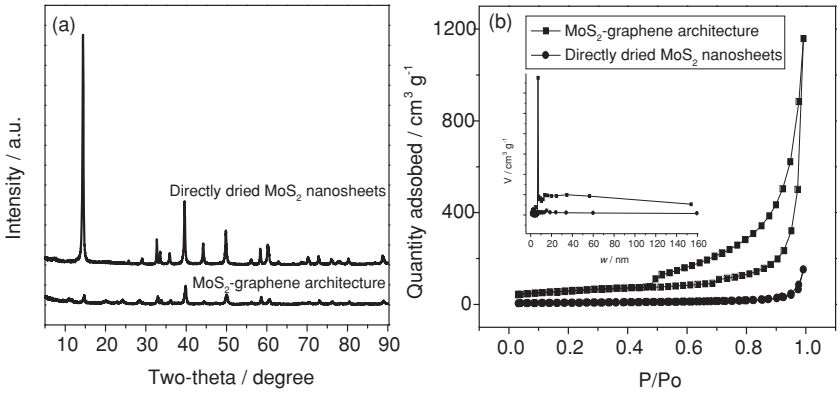

Figure 4. Structural characteristics of 3D MoS_2-graphene architectures. Typical a) XRD patterns and b) nitrogen adsorption/desorption isotherms of MoS_2-graphene architecture (84%) and directly dried MoS_2 nanosheets. The isotherm in (b) confirms the porous structure (inset: pore size distribution) of MoS_2-graphene architecture with a BET surface areas of 205 $m^2\ g^{-1}$.

2.2. Electrochemical Properties of MoS_2 and Graphene Sheets Co-Constructed 3D Architectures

To investigate the electrochemical properties of as-prepared MoS-$_2$-graphene architectures, cyclic voltammetry (CV) measurements were first conducted at a scanning rate of 0.1 mV s^{-1} over the potential range from 3.0 to 0.01 V. As shown in **Figure 5**, during the first scanning cycle, there are three reduction peaks and one oxidation peak for MoS-$_2$-graphene architecture. The first dominant reduction peak at 1.04 V is commonly assigned to Li insertion into MoS_2, forming Li_xMoS_2.[35] And the second pronounced reduction peak at 0.46 V is ascribed to the

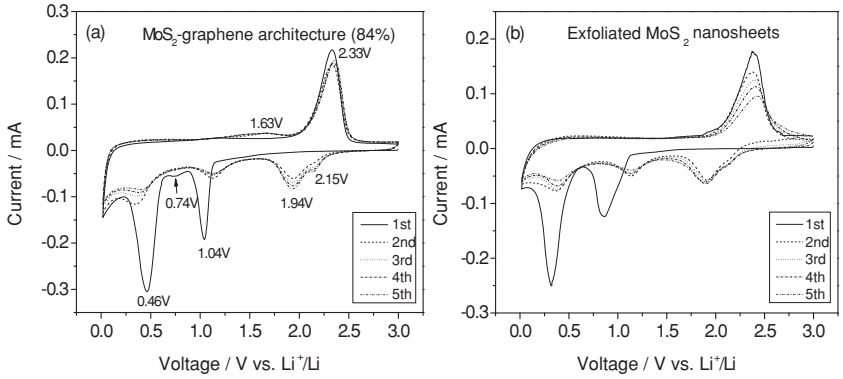

Figure 5. Cyclic voltammograms of a) MoS_2-graphene architecture and b) exfoliated MoS_2 nanosheets at a scanning rate of 0.1 mV s^{-1}, respectively.

reduction of Li_xMoS_2 to Mo metal and Li_2S via a conversion reaction.[36] The strong oxidation peak at 2.33 V can be attributed to the oxidation of Li_2S into sulfur (S) according to the literature.[35] Thus, after the first cycle, the electrode can be regarded as a mixture of S, Mo graphene instead of the original MoS_2 -graphene composite. Accordingly, the reduction peak at ≈2.0 V is indicative of the formation of Li_2S. Further investigation reveals that at 2.15 V and 1.94 V, respectively, which agree well with the kinetics of the conversion from S8 to polysulfides and then to Li_2S.[35,37] The other two reduction peaks occurring at 1.12 V and 0.37 V are ascribed to the association of Li with Mo. The weak reduction peak at 0.74 V and oxidation peak at 1.63 V should be attributed to the reversible lithium storage on graphene layers since they are absent in the CV curves of exfoliated MoS_2 sheets (Figure 5b), demonstrating both MoS_2 and graphene sheets in the composites are electrochemically active materials for lithium storage.

The electrochemical performances of 3D MoS_2-graphene architectures were further systematically evaluated by galvanostatic discharge (lithium insertion)–charge (lithium extraction) measurements. Remarkably, a very high reversible capacity of 1220 mAh g^{-1} is achieved in the initial cycles at a current density of 74 mA g^{-1}, in the case of MoS_2-graphene architecture with the MoS_2 content of 84% (**Figure 6**). Even after 30 cycles, both discharge and charge capacities of this architecture are stabile at about 1216 mAh g^{-1}, delivering nearly 100% capacity retention (Figure 6c). This result is in stark contrast to the exfoliated MoS_2 nanosheets, bulk MoS_2 and MoS_2-graphene architectures with the content of more than 84% (Supporting Information Figure S6), which show continuous and progressive capacity decay along with cycling processes. Associated with their morphology and structure analysis, it is known that the cycling performance of MoS_2-graphene architectures is strongly dependent on the dispersion degree of MoS_2 nanosheets in the

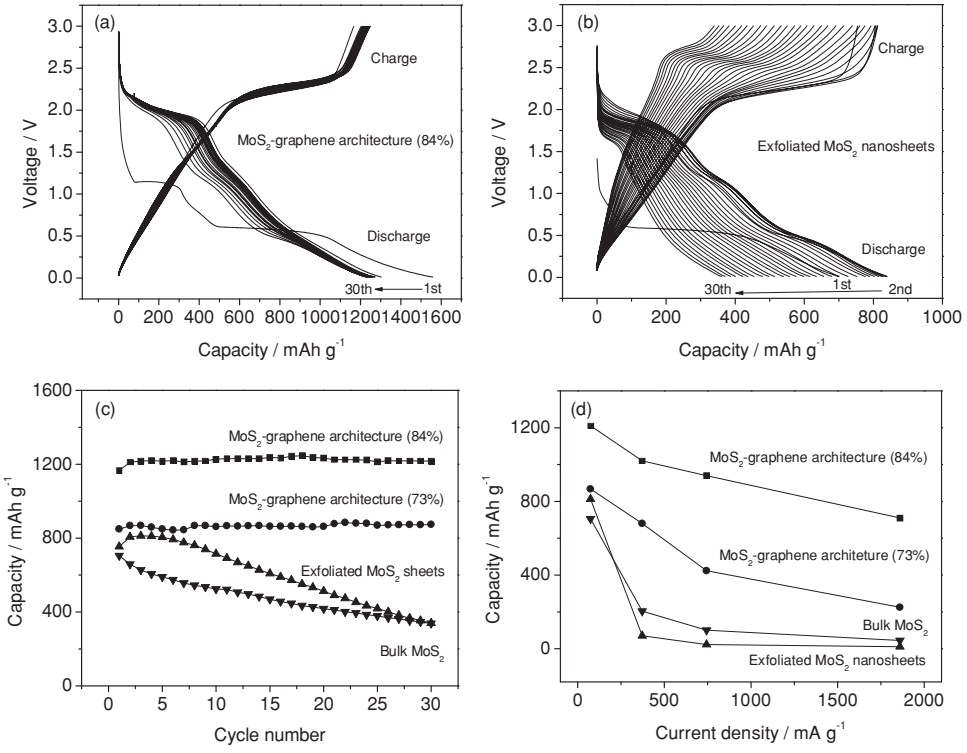

Figure 6. Electrochemical performance of 3D MoS_2-graphene architectures for high-performance lithium storage. Galvanostatic discharge–charge profiles of a) 3D MoS_2-graphene architecture (84%) and b) MoS_2 nanosheets at a current density of 74 mA g^{-1}. Comparisons of c) cycling performances and d) rate capabilities of 3D MoS_2-graphene architectures, MoS_2 nanosheets and bulk MoS_2.

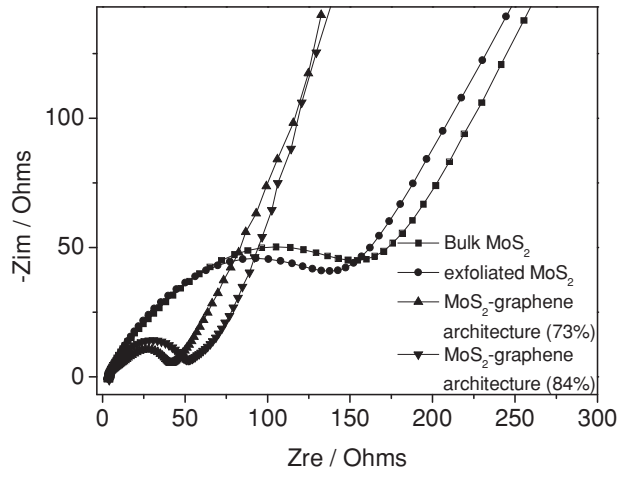

Figure 7. Nyquist plots of 3D MoS_2-graphene architectures, MoS_2 nanosheets and bulk MoS_2 electrodes obtained by applying a sine wave with amplitude of 5.0 mV over the frequency range 100 kHz–0.01 Hz.

graphene matrix since graphene can not only efficiently prevent the aggregation of exfoliated MoS_2 nanosheets but can also maintain the high electric conductivity of overall electrode. More importantly, MoS_2-graphene architectures exhibit good high-rate performance. For example, the reversible capacities of the 3D architectures with the MoS_2 content of 84% are still as high as 939 and 711 mAh g^{-1}, as increasing the current densities to 744 and 1860 mA g^{-1} (Figure 6d and Supporting Information Figure S7, respectively). Clearly, the high-rate performances of 3D MoS_2-graphene architectures are much better than most reported MoS_2-based hybrids such as MoS_2-carbon nanotubes[38] and MoS_2/poly(ethylene oxide) composites,[35] although they are still lower than that of pure graphene films.[39]

To gain more insight, AC impedance measurements of the MoS_2-graphene architectures, MoS_2 nanosheets and bulk MoS_2 electrodes were performed after 30 cycles. Their Nyquist plots (**Figure 7**) show that the diameter of the semicircles for MoS_2-graphene architecture electrodes in the high-medium frequency region are much smaller than those of exfoliated MoS_2 nanosheets and bulk MoS_2 electrodes, suggesting that MoS_2-graphene architectures possess much lower contact and charge-transfer resistances. The exact kinetic differences among the studying electrodes were inspected by modeling AC impedance spectra based on the modified Randles equivalent circuit[30] (Supporting Information Figure S8) and summarized in Supporting Information Table S1. The values of the Ohmic resistance and charge-transfer resistance are 28.5 and 8.4 Ω, respectively, for MoS_2-graphene architecture (85%), which are significantly lower than those of MoS_2 nanosheets (90.4 and 19.3 Ω) and bulk MoS_2 (88.5 and 20.2 Ω). Correspondingly, the exchange-current density i_0 of MoS_2-graphene architecture (3.9 mA cm^{-2}) is twice as high as those of directly dried MoS_2 nanosheets (1.7 mA cm^{-2}) and bulk MoS_2 (1.6 mA cm^{-2}), implying much higher electrochemical activity of 3D architectures with respect to lithium storage.

3. Conclusions

In summary, we have developed a bottom-up approach to successfully fabricate 3D hybrid architectures from 2D MoS_2 and graphene oxide nanosheets. The resulting 3D MoS_2-graphene architectures possess high surface area, multilevel porous structure and high electrical conductivity, facilitating the diffusion of both lithium and electrons during lithium storage. Hence, remarkable electrochemical performances including highly reversible capacity and excellent cycling performance are achieved. We believe that such a simple and efficient assembly protocol will provide a new pathway for the large-scale production of various 3D functional architectures by employing different nanosheets with broad applications in electronics, fuel cells, supercapacitors, and lithium ion batteries.

4. Experimental Section

MoS_2 nanosheets were fabricated by liquid exfoliation of commercially available g MoS_2 (Aldrich) powders via a sonication in mixed IPA/water solvents. In a typical synthesis, 30 mg of MoS_2 powder was added into 25 ml flask. 10 mL of IPA/water (45 vol%) mixed solvent was added into above flask as dispersion solvent. The sealed flask was sonicated for 10 h, and then the dispersion was centrifuged at 2000 rpm for 10 min to remove aggragates. Graphene oxide (GO) nanosheets were synthesized from natural graphite flakes by a modified Hummers method,[29] the details of which were described elsewhere.[3] 3D architectures were synthesized by a combined hydrothermal assembly and chemical reduction processes. In a typical procedure, a 10 mL of GO (2 mg mL^{-1}) aqueous dispersion were mixed with 5 mL of IPA suspension of MoS_2 nanosheets with different concentrations by sonication for 2 h. The resulting stable suspension, sealed in a Telfon-lined autoclave, was hydrothermally treated at 180 °C for 12 h. Finally, the as-prepared sample was chemically reduced and critical point- or freeze- dried.

The morphology and microstructure of the samples were systematically investigated by SEM (JEOL 6500), TEM (JEOL 2010), HRTEM (Field Emission JEOL 2100), AFM (Digital Instrument Nanoscope IIIA), XPS (PHI Quantera X-ray photoelectron spectrometer) and XRD (Rigaku D/Max Ultima II Powder X-ray diffractometer) measurements. Nitrogen sorption isotherms and BET surface area were measured at 77 K with a Quantachrome Autosorb-3B analyzer (USA). Electrochemical experiments were carried out in 2032 coin-type cells. The working electrodes were prepared by mixing our samples, carbon black (Super-P), and poly(vinyl difluoride) (PVDF) at a weight ratio of 80:10:10 and pasted on pure copper foil (99.6%, Goodfellow). The mass loading of the electrode materials on copper foil is about 1.5 mA cm^{-2}. Pure lithium foil (Aldrich) was used as the counter electrode. The electrolyte consisted of a solution of 1 M $LiPF_6$ in ethylene carbonate (EC)/dimethyl carbonate (DMC)/diethyl carbonate (DEC) (1:1:1 by volume) obtained from MTI Corporation. The cells were assembled in an argon-filled glovebox with the concentrations of moisture and oxygen below 0.1 ppm. The electrochemical performance was tested at various current densities in the voltage range of 0.01–3.00 V. The impedance spectra were recorded by applying a sine wave with amplitude of 5.0 mV over the frequency range from 100 kHz to 0.01 Hz. Fitting of the impedance spectra to the proposed equivalent circuit was performed by the code Zview.

Supporting Information

Supporting Information is available from the Wiley Online Library or from the author.

Acknowledgements

This work was financially supported by U. S. Army Research Office through the MURI grant (W911NF-11-1-0362) entitled,"Atomic Layers of Nitrides, Oxides, and Sulfides". S. Y., R.V. and P. M. A. also acknowledge funding sponsorship from the U.S. Air Force Office of Scientific Research for the MURI grant (FA9550-12-1-0035) entitled,"Synthesis and Characterization of 3-D Carbon Nanotube Solid Networks".

Received: March 8, 2013
Revised: April 18, 2013
Published online: June 25, 2013

[1] K. S. Novoselov, Z. Jiang, Y. Zhang, S. V. Morozov, H. L. Stormer, U. Zeitler, J. C. Maan, G. S. Boebinger, P. Kim, A. K. Geim, *Science* **2007**, *315*, 1379.
[2] M. Choi, K. Na, J. Kim, Y. Sakamoto, O. Terasaki, R. Ryoo, *Nature* **2009**, *461*.
[3] S. B. Yang, X. L. Feng, L. Wang, K. Tang, J. Maier, K. Müllen, *Angew. Chem. Int. Ed.* **2010**, *49*, 4795.
[4] S. B. Yang, X. L. Feng, X. C. Wang, K. Müllen, *Angew. Chem. Int. Ed.* **2011**, *50*, 5339.
[5] B. Luo, B. Wang, X. L. Li, Y. Y. Jia, M. H. Liang, L. J. Zhi, *Adv. Mater.* **2012**, *24*, 3538.
[6] S. B. Yang, R. E. Bachman, X. L. Feng, K. Müllen, *Acc. Chem. Res.* **2013**, *46*, 116.
[7] Y. W. Zhu, S. Murali, M. D. Stoller, K. J. Ganesh, W. W. Cai, P. J. Ferreira, A. Pirkle, R. M. Wallace, K. A. Cychosz, M. Thommes, D. Su, E. A. Stach, R. S. Ruoff, *Science* **2011**, *332*, 1537.
[8] F. Yavari, Z. P. Chen, A. V. Thomas, W. C. Ren, H. M. Cheng, N. Koratkar, *Sci. Rep.* **2011**, *1*, 166.
[9] W. Gao, N. Singh, L. Song, Z. Liu, A. L. M. Reddy, L. J. Ci, R. Vajtai, Q. Zhang, B. Q. Wei, P. M. Ajayan, *Nat. Nanotechnol.* **2011**, *6*, 496.
[10] Z. S. Wu, Y. Sun, Y. Z. Tan, S. B. Yang, X. L. Feng, K. Mullen, *J. Am. Chem. Soc.* **2012**, *134*, 19532.
[11] A. K. Geim, *Science* **2009**, *324*, 1530.
[12] X. Du, I. Skachko, A. Barker, E. Y. Andrei, *Nat. Nanotechnol.* **2008**, *3*, 491.
[13] D. A. Abanin, S. V. Morozov, L. A. Ponomarenko, R. V. Gorbachev, A. S. Mayorov, M. I. Katsnelson, K. Watanabe, T. Taniguchi, K. S. Novoselov, L. S. Levitov, A. K. Geim, *Science* **2011**, *332*, 328.
[14] J. Rafiee, X. Mi, H. Gullapalli, A. V. Thomas, F. Yavari, Y. F. Shi, P. M. Ajayan, N. A. Koratkar, *Nat. Mater.* **2012**, *11*, 217.
[15] L. Song, L. J. Ci, H. Lu, P. B. Sorokin, C. H. Jin, J. Ni, A. G. Kvashnin, D. G. Kvashnin, J. Lou, B. I. Yakobson, P. M. Ajayan, *Nano Lett.* **2010**, *10*, 3209.
[16] L. Ci, L. Song, C. H. Jin, D. Jariwala, D. X. Wu, Y. J. Li, A. Srivastava, Z. F. Wang, K. Storr, L. Balicas, F. Liu, P. M. Ajayan, *Nat. Mater.* **2010**, *9*, 430.
[17] M. Osada, T. Sasaki, *Adv. Mater.* **2012**, *24*, 210.
[18] J. N. Coleman, M. Lotya, A. O'Neill, S. D. Bergin, P. J. King, U. Khan, K. Young, A. Gaucher, S. De, R. J. Smith, I. V. Shvets, S. K. Arora, G. Stanton, H. Y. Kim, K. Lee, G. T. Kim, G. S. Duesberg, T. Hallam, J. J. Boland, J. J. Wang, J. F. Donegan, J. C. Grunlan, G. Moriarty, A. Shmeliov, R. J. Nicholls, J. M. Perkins, E. M. Grieveson, K. Theuwissen, D. W. McComb, P. D. Nellist, V. Nicolosi, *Science* **2011**, *331*, 568.
[19] B. Luo, Y. Fang, B. Wang, J. S. Zhou, H. H. Song, L. J. Zhi, *Energy Environ. Sci.* **2012**, *5*, 5226.
[20] K. S. Novoselov, A. K. Geim, S. V. Morozov, D. Jiang, Y. Zhang, S. V. Dubonos, I. V. Grigorieva, A. A. Firsov, *Science* **2004**, *306*, 666.
[21] K. S. Novoselov, A. K. Geim, S. V. Morozov, D. Jiang, M. I. Katsnelson, I. V. Grigorieva, S. V. Dubonos, A. A. Firsov, *Nature* **2005**, *438*, 197.
[22] X. S. Li, W. W. Cai, J. H. An, S. Kim, J. Nah, D. X. Yang, R. Piner, A. Velamakanni, I. Jung, E. Tutuc, S. K. Banerjee, L. Colombo, R. S. Ruoff, *Science* **2009**, *324*, 1312.
[23] C. Berger, Z. M. Song, X. B. Li, X. S. Wu, N. Brown, C. Naud, D. Mayou, T. B. Li, J. Hass, A. N. Marchenkov, E. H. Conrad, P. N. First, W. A. de Heer, *Science* **2006**, *312*, 1191.
[24] P. W. Sutter, J. I. Flege, E. A. Sutter, *Nat. Mater.* **2008**, *7*, 406.
[25] Y. Hernandez, V. Nicolosi, M. Lotya, F. M. Blighe, Z. Y. Sun, S. De, I. T. McGovern, B. Holland, M. Byrne, Y. K. Gun'ko, J. J. Boland, P. Niraj, G. Duesberg, S. Krishnamurthy, R. Goodhue, J. Hutchison, V. Scardaci, A. C. Ferrari, J. N. Coleman, *Nat. Nanotechnol.* **2008**, *3*, 563.
[26] D. Li, M. B. Muller, S. Gilje, R. B. Kaner, G. G. Wallace, *Nat. Nanotechnol.* **2008**, *3*, 101.
[27] A. S. Arico, P. Bruce, B. Scrosati, J. M. Tarascon, W. Van Schalkwijk, *Nat. Mater.* **2005**, *4*, 366.
[28] P. G. Bruce, B. Scrosati, J. M. Tarascon, *Angew. Chem. Int. Ed.* **2008**, *47*, 2930.
[29] W. S. Hummers, R. E. Offeman, *J. Am. Chem. Soc.* **1958**, *80*, 1339.
[30] S. B. Yang, X. L. Feng, S. Ivanovici, K. Müllen, *Angew. Chem. Int. Ed.* **2010**, *49*, 8408.
[31] A. Fasolino, J. H. Los, M. I. Katsnelson, *Nat. Mater.* **2007**, *6*, 858.
[32] K. X. Sheng, Y. Q. Sun, C. Li, W. J. Yuan, G. Q. Shi, *Sci. Rep.* **2012**, *2*, 247.
[33] H. P. Cong, X. C. Ren, P. Wang, S. H. Yu, *ACS Nano* **2012**, *6*, 2693.
[34] Y. X. Xu, K. X. Sheng, C. Li, G. Q. Shi, *ACS Nano* **2010**, *4*, 4324.
[35] J. Xiao, X. J. Wang, X. Q. Yang, S. D. Xun, G. Liu, P. K. Koech, J. Liu, J. P. Lemmon, *Adv. Funct. Mater.* **2011**, *21*, 2840.
[36] Q. Wang, J. H. Li, *J. Phys. Chem. C* **2007**, *111*, 1675.
[37] X. L. Ji, K. T. Lee, L. F. Nazar, *Nat. Mater.* **2009**, *8*, 500.
[38] S. J. Ding, J. S. Chen, X. W. Lou, *Chem. Eur. J.* **2011**, *17*, 13142.
[39] R. Mukherjee, A. V. Thomas, A. Krishnamurthy, N. Koratkar, *ACS Nano* **2012**, *6*, 7867.